Characterisation of conductivity of the $(Ce_xY_{0.2-x})Sc_{0.6}Zr_{3.2}O_{8-\delta}$ $(0 \leq x \leq 0.2)$ system and composition $Ce_{0.04}Y_{0.02}Sc_{0.67}Zr_{3.27}O_{7.66}$ as function of time

(Caracterização da condutividade do sistema $(Ce_xY_{0,2-x})Sc_{0,6}Zr_{3,2}O_{8-\delta}$ $(0 \leq x \leq 0,2)$ e da composição $Ce_{0,04}Y_{0,02}Sc_{0,67}Zr_{3,27}O_{7,66}$ em função do tempo)

E. de Carvalho, J. T. S Irvine
School of Chemistry, University of St Andrews, North Haugh, St. Andrews, Fife, KY169ST, Scotland, United Kingdom

Abstract

The conductivity behaviour of the $(Ce_xY_{0.2-x})Sc_{0.6}Zr_{3.2}O_{8-\delta}$ $(0 \leq x \leq 0.2)$ system and composition $Ce_{0.04}Y_{0.02}Sc_{0.67}Zr_{3.27}O_{7.66}$ have been investigated as function of time using impedance spectroscopy. All samples were prepared by sol-gel and combustion process, sintered at 1500 °C for 12 h and the densities obtained were between 92 and 97%. The electrical measurements were performed at 600 °C. The conductivity values were fairly stable during the first 1800 h of the experiment but after this time the conductivity decreases. For some compositions of the system a semi-circle is detected through time, with capacitance values of an order of magnitude lower, 10^{-8} F/cm. This semi-circle becomes well defined with time. After the experiment, SEM pictures show that grain boundary is well defined and an increase of pore inside grains, in some cases the surface is damaged showing cracks and fissures indicating microstructure deterioration.
Keywords: scandia-zirconia, ac impedance, ageing.

Resumo

O comportamento da condutividade do sistema $(Ce_xY_{0.2-x})Sc_{0,6}Zr_{3,2}O_{8-\delta}$ $(0 \leq x \leq 0,2)$ e da composição $Ce_{0,04}Y_{0,02}Sc_{0,67}Zr_{3,27}O_{7,66}$, foi investigado em função do tempo usando espectroscopia de impedância. Todas as amostras foram preparadas pelo processo de sol gel e combustão combinados, sinterizadas a 1500 ºC durante 12 h e as densidades obtidas estão entre 92 e 97%. Esta experiência foi executada a 600 °C. Os valores da condutividade apresentaram-se relativamente estáveis durante as primeiras 1800 h da experiência mas depois deste tempo de funcionamento a condutividade decresceu. Para algumas composições do sistema um semi-circulo apareceu ao longo do tempo, com valores de capacidade com ordem de grandeza 10^{-8} F/cm. Estes semi-círculos tornam-se melhor definidos com o tempo. Depois desta experiência as micrografias de microscopia eletrônica de varredura destas amostras mostram que a fronteira de grão é bem definida e que ocorreu um aumento de porosidade, e em algumas amostras a superfície ficou danificada mostrando fissuras e trincas na superfície indicando deterioração na microestrutura.
***Palavras-chave**: zircônia-escândia, impedância ac, envelhecimento.*

INTRODUCTION

Scandia-stabilised zirconia (SSZ) is probably the most promising material to be used as an electrolyte for intermediate temperatures due to its high ionic conductivity, stability under reducing and oxidising atmospheres and low electronic conductivity. The ionic conductivity of SSZ is three time higher than 8YSZ, at 800 °C, which enables SSZ to work at lower temperatures [1-4]. The degradation of conductivity is likely to occur due to a change in the nanostructure of the system [5-7]. This means that a change in the defect structure and nearest environment of the ions occurs. Zhang *et al*. [8] state that there are four possible microstructural changes, which are responsible for the decrease in conductivity of doped zirconia electrolytes caused by ageing: (1) precipitation of long range ordered phases; (2) formation and precipitation of tetragonal phase in the cubic grains; (3) segregation of dopant-rich layer near grain boundaries and triple points and (4) trapping of oxygen vacancies ($V_O^{\cdot\cdot}$) towards dopant cations with time due to the Coulombic force, short range ordering of oxygen vacancies. In point (2) the formation and precipitation occur as a result of "growing" of the metastable tetragonal (t or t') or cubic phase in the ZrO_2-Y_2O_3 system and the t'-phase in the ZrO_2-Sc_2O_3 system into low-dopant tetragonal and dopant-rich cubic phases [7, 9, 10]. Phase transformation of the zirconia electrolytes can be caused, not only by the type of dopants and dopant concentrations, but also by ageing.

EXPERIMENTAL

The powders were prepared by a sol–gel combustion method [12]. Scandia powders (TTE Metals, 99.9% purity) were dissolved in nitric acid (Fisher Scientific, 70%) and hydrogen peroxide (Fisher Scientific, N30% wv). Separately, cerium (III) nitrate hexahydrate (Aldrich, 99% purity),

yttrium nitrate hexahydrate (Aldrich, 99.9%) and zirconia acetylacetonate (IV) (Aldrich, 98% purity) were dissolved in distilled water. The first solution was added to the second; after the two solutions were mixed, glycine was introduced. Ammonia was introduced until the pH was approximately 6. The temperature was increased to 150 °C and maintained constant until the gel was formed. After formation of the gel the temperature was increased to 270 °C, so that the gel burned off. The powders were calcined for 3 h at 400 °C with a heating ramp of 1 °C/min. After rapidly cooling down to room temperature, the powder was ground. The crystal structure of the calcined powders was verified by XRD, using a Phillips diffractometer (20–90 2θ, step size 90 0.02°, 2θ, Cukα radiation). The zirconia powders were milled using a Fritsch Planetary Ball Mill "pulverisette 7" with zirconia containers and zirconia balls on a suspension in acetone and triton QS-44 (phosphate ester, acid form, Sigma Chemical) 4% of powder weight. Dried powders were pressed uniaxially at 75 MPa and isostatically at 200 MPa into pellets with a diameter of 13 mm and thickness of 0.6–1.0 mm. The pellets were sintered at 1500 °C and removed from the furnace at 1000 °C to cool down to room temperature.

The electrodes used to measure ac impedance were made of platinum, which was brushed on the base and the top of the pellet surface. After drying the platinum paste, the pellets were sintered at 900 °C, for 30 minutes. The experiment was performed as follow: pellets were introduced in the furnace and heated up to 600 °C, at the rate of 10 ºC/min, and then held at 600 °C. For every measurement, pellets are removed from the furnace and left in air to cool down. One hour before the measurement, pellets are placed in the jig and inside a furnace at 600 °C. The impedance measurements are performed by means of a frequency response analyzer HP Hewlett-Packard, 4192A LF. The frequency range is 13 MHz-5 Hz and the effective ac voltage amounted to 20 mV. After the end of these experiments, pellets were cut, polished and observed in the SEM.

RESULTS AND DISCUSSION

Pellets used in this experiment were sintered at 1500 °C for 12 h. All densities are above 92%, the highest achieved is for the composition $Ce_{0.1}Y_{0.1}Sc_{0.6}Zr_{3.2}O_{7.65}$, which is 97%, as shown in Table I.

The X-ray diffraction pattern (Fig. 1) of the $(Ce_xY_{0.2-x})Sc_{0.6}Zr_{3.2}O_{8-\delta}$ ($0 \leq x \leq 0.2$) system and composition $Ce_{0.04}Y_{0.02}Sc_{0.67}Zr_{3.27}O_{7.66}$ calcined at 400 ºC for 3 h showed a presence of a single phase with a cubic fluorite-type structure, Fm3m space group.

Fig. 2 summarises the changes in the conductivity behaviour against time, performed at 600 ºC for almost 4500 h, for all compositions. The shaded area is to stand out the degradation in conductivity of the pellets.

For the first 1800 h of the experiment, there is no significant variation of the conductivity, although some oscillation can be observed. The stability of the conductivity is in agreement with results from Haering *et al* [9, 11]. After 1800 h, shaded area in Fig. 2, all compositions decrease their conductivity, until time equal 2896 h. During this experiment a power failure occurred at approximately 3500 h and last for 36 h, therefore the last measurement at 4240 h was excluded from discussion, as the conductivity values increased instead of the expected decrease. Composition $Ce_{0.20}Sc_{0.6}Zr_{3.2}O_{7.70}$ (in orange) has the highest conductivity and also has the highest amount of ceria, on the other hand, the composition with no ceria content (in red) has the lowest conductivity values. There are no measurements for the pellets from the composition with no ceria, after 1729 h, because they were damaged. The values for total conductivity, for the

Table I - Density of pellets from the system $Ce_xY_{0.2-x}Sc_{0.6}Zr_{3.2}O_{8-d}$ ($0 \leq x \leq 0.2$) and from composition $Ce_{0.04}Y_{0.02}Sc_{0.67}Zr_{3.27}O_{7.66}$ and nomenclature used.
[Tabela I - Densidade das pastilhas do sistema $Ce_xY_{0,2-x}Sc_{0,6}Zr_{3,2}O_{8-d}$ ($0 \leq x \leq 0,2$) e da composição $Ce_{0,04}Y_{0,02}Sc_{0,67}Zr_{3,27}O_{7,66}$ e a nomenclatura usada.]

Composition	Theoretical density, g/cm³	Sample density, g/cm³	% Density	Nomenclature
$Ce_{0.04}Y_{0.02}Sc_{0.67}Zr_{3.27}O_{7.66}$	5.708	5.418	95	Initial
$Y_{0.2}Sc_{0.6}Zr_{3.2}O_{7.60}$	5.699	5.261	92	x=0
$Ce_{0.04}Y_{0.16}Sc_{0.6}Zr_{3.2}O_{7.62}$	5.691	5.334	94	x=0.04
$Ce_{0.08}Y_{0.12}Sc_{0.6}Zr_{3.2}O_{7.64}$	5.725	5.302	93	x=0.08
$Ce_{0.1}Y_{0.1}Sc_{0.6}Zr_{3.2}O_{7.65}$	5.732	5.551	97	x=0.10
$Ce_{0.12}Y_{0.08}Sc_{0.6}Zr_{3.2}O_{7.66}$	5.771	5.339	93	x=0.12
$Ce_{0.16}Y_{0.04}Sc_{0.6}Zr_{3.2}O_{7.68}$	5.779	5.430	94	x=0.16
$Ce_{0.20}Sc_{0.6}Zr_{3.2}O_{7.70}$	5.798	5.326	92	x=0.20

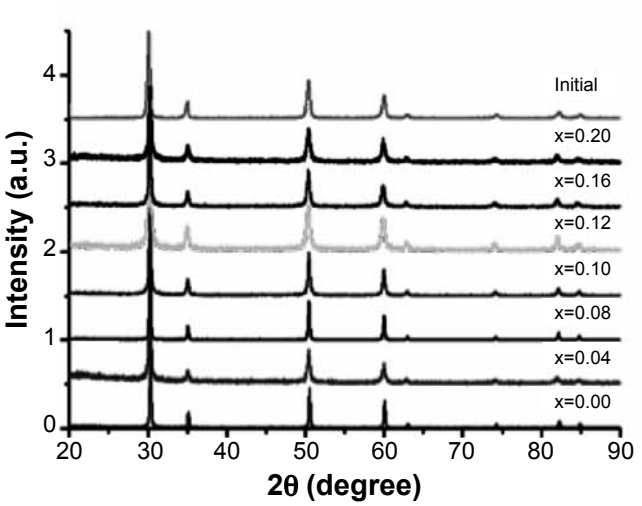

Figure 1: X-ray diffraction patterns of the system $Ce_xY_{0.2-x}Sc_{0.6}Zr_{3.2}O_{8-\delta}$ ($0 \le x \le 0.2$), and the composition $Ce_{0.04}Y_{0.02}Sc_{0.67}Zr_{3.27}O_{7.66}$, calcined at 400 °C for 3 h.
[Figura 1: DRX dos pós do sistema $Ce_xY_{0,2-x}Sc_{0,6}Zr_{3,2}O_{8-\delta}$ ($0 \le x \le 0,2$), e da composição $Ce_{0,04}Y_{0,02}Sc_{0,67}Zr_{3,27}O_{7,66}$, calcinado 400 °C durante 3 h.]

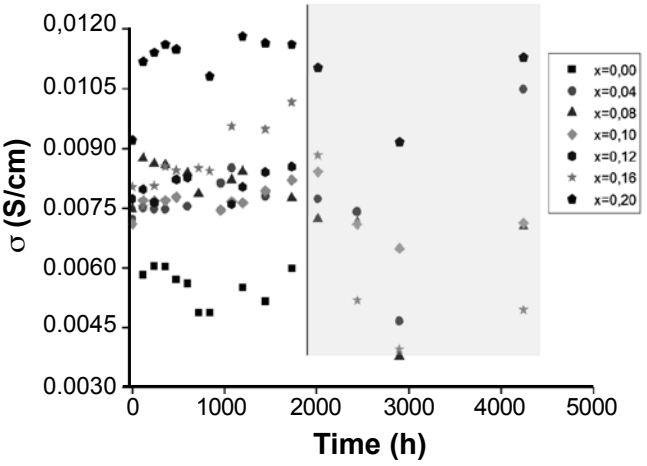

Figure 2: Variation of total conductivity with time, for compositions of the system $Ce_xY_{0.2-x}Sc_{0.6}Zr_{3.2}O_{8-\delta}$ ($0 \le x \le 0.2$) and the composition $Ce_{0.04}Y_{0.02}Sc_{0.67}Zr_{3.27}O_{7.66}$, at 600 °C.
[Figura 2: Variação da condutividade total com o tempo, para o sistema $Ce_xY_{0,2-x}Sc_{0,6}Zr_{3,2}O_{8-\delta}$ ($0 \le x \le 0,2$) e para a composição $Ce_{0,04}Y_{0,02}Sc_{0,67}Zr_{3,27}O_{7,66}$, a 600 °C.]

first measurement, time equals 0 h, are lower than for the second measurement, after 480 h, except for compositions $Y_{0.2}Sc_{0.6}Zr_{3.2}O_{7.60}$ and $Ce_{0.16}Y_{0.04}Sc_{0.6}Zr_{3.2}O_{7.68}$, Fig. 2. One possible explanation is that the first measurement could have been performed at a slightly lower temperature than for the remaining part of the experiment.

Table II shows the values for conductivity of the first measurement for 0 h, measurement for 480 h, to have stable temperature conditions, for comparison. The fourth column presents values for conductivity from experiments of temperature variation [12].

For all compositions there is a slight increase in conductivity after 480 h when compared with conductivity values for 0 h, except for compositions $Y_{0.2}Sc_{0.6}Zr_{3.2}O_{7.60}$. This can reinforce the idea of the first measurement, for the ageing experiment, being performed at temperatures slightly below 600 °C and the difference in conductivity, in some compositions, can also be due to the better ionic conductivity of the samples.

Observing Fig. 3 and Table III, one can say that the resistance decreases, from the beginning of the experiment to 960 h. From 960 h until 2440 h, the resistance increases; when the measurement is performed at 2896 h there is an increase in resistance and in addition there is the appearance of a semi-circle, which provides values for the bulk and grain boundary resistance, shown in Table III.

Table II - Conductivity of the first measurement for the ageing experiment and conductivity of other samples for the same composition.
[Tabela II - Condutividade da primeira medida da experiencia de envelhecimento e condutividade de outras amostras, com a mesma composição, para a mesma temperatura.]

Composition	Conductivityafter 0 h, S/cm	Conductivity after 480 h, S/cm	Conductivity, S/cm [12]
$Ce_{0.04}Y_{0.02}Sc_{0.67}Zr_{3.27}O_{7.66}$	0.0100	0.0093	0.016
$Y_{0.2}Sc_{0.6}Zr_{3.2}O_{7.60}$	0.0071	0.0057	0.010
$Ce_{0.04}Y_{0.16}Sc_{0.6}Zr_{3.2}O_{7.62}$	0.0072	0.0075	0.008
$Ce_{0.08}Y_{0.12}Sc_{0.6}Zr_{3.2}O_{7.64}$	0.0075	0.0085	0.010
$Ce_{0.1}Y_{0.1}Sc_{0.6}Zr_{3.2}O_{7.65}$	0.0071	0.0078	0.006
$Ce_{0.12}Y_{0.08}Sc_{0.6}Zr_{3.2}O_{7.66}$	0.0077	0.0082	0.009
$Ce_{0.16}Y_{0.04}Sc_{0.6}Zr_{3.2}O_{7.68}$	0.0080	0.0084	0.014
$Ce_{0.20}Sc_{0.6}Zr_{3.2}O_{7.70}$	0.0092	0.0115	0.010

AC impedance spectra of $Ce_{0.04}Y_{0.16}Sc_{0.6}Zr_{3.2}O_{7.62}$

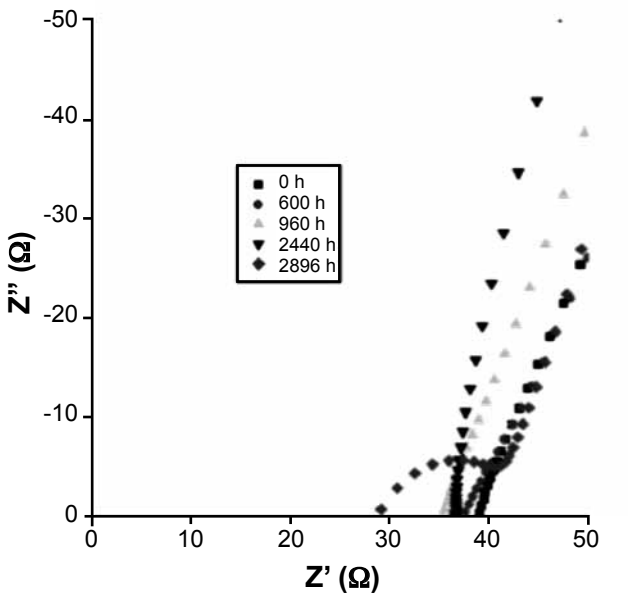

Figure 3: Impedance spectra plot from the composition $Ce_{0.04}Y_{0.16}Sc_{0.6}Zr_{3.2}O_{7.62}$, at 600 °C.
[Figura 3: Espectros de impedância para a composição $Ce_{0,04}Y_{0,16}Sc_{0,6}Zr_{3,2}O_{7,62}$, a 600 °C.]

AC impedance spectra of $Ce_{0.16}Y_{0.04}Sc_{0.6}Zr_{3.2}O_{7.68}$

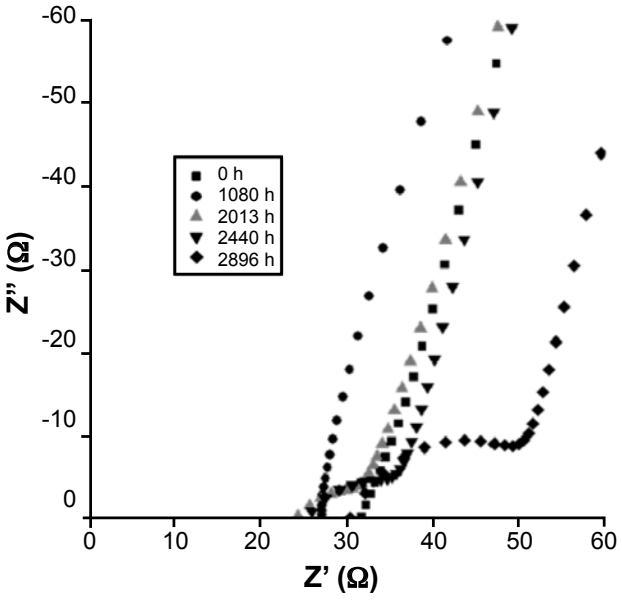

Figure 4: Impedance spectra plot of the composition $Ce_{0.16}Y_{0.04}Sc_{0.6}Zr_{3.2}O_{7.68}$, at 600 °C.
[Figura 4: Espectros de impedância da composição $Ce_{0,16}Y_{0,04}Sc_{0,6}Zr_{3,2}O_{7,68}$, a 600 °C.]

Table III - Bulk resistance, grain boundary resistance and total resistance and capacitance correspondent to the semi-circle.
[Tabela III - Resistência do grão, resistência da fronteira de grão e resistência total, e capacidade correspondente ao semi-circulo.]

Time, h	bulk resistance ρ_b (Ohm.cm)	grain boundary resistance ρ_{gb} (Ohm.cm)	total resistance ρ_t (Ohm.cm)	Capacitance, (F/cm)
0	-	-	38.88	-
600	-	-	37.41	-
960	-	-	34.96	-
2440	-	-	36.62	-
2896	40.49	16.52	57.01	1.31×10^{-8}

Table IV - Bulk resistance, grain boundary resistance and total resistance and capacitance correspondent to the semi-circle.
[Tabela IV - Resistência do grão, resistência da fronteira de grão e resistência total e capacidade correspondente ao semi-circulo.]

Time, h	bulk resistance ρ_b (Ohm.cm)	grain boundary resistance ρ_{gb} (Ohm.cm)	total resistance ρ_t (Ohm.cm)	Capacitance (F/cm)
0	-	-	31.59	-
1080	-	-	27.09	-
2013	22.88	20.11	42.99	4.73×10^{-8}
2440	24.29	20.50	44.79	2.01×10^{-8}
2896	30.25	28.05	58.30	9.12×10^{-9}

AC impedance spectra of $Ce_{0.20}Sc_{0.6}Zr_{3.2}O_{7.70}$

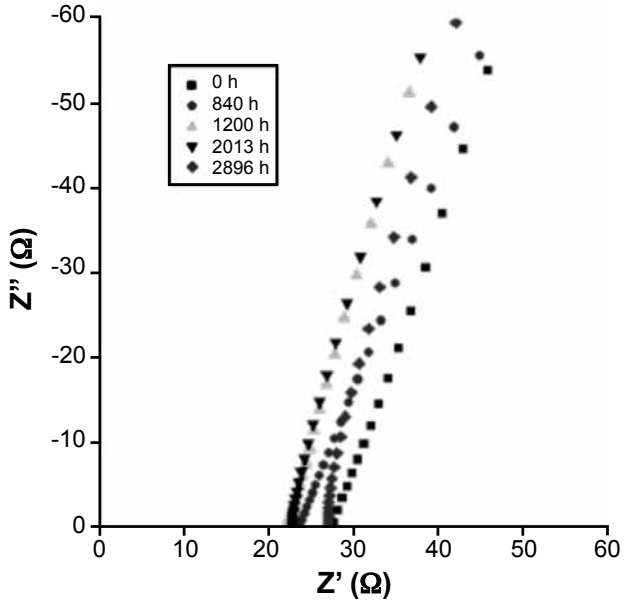

Figure 5: Impedance spectra plot of the composition $Ce_{0.20}Sc_{0.6}Zr_{3.2}O_{7.70}$, at 600 °C.
[Figura 5: Espectros de impedância da composição $Ce_{0.20}Sc_{0.6}Zr_{3.2}O_{7.70}$, a 600 °C.]

Table V - Total resistance for different times.
[Tabela V - Resistência total para os diferentes tempos.]

Time, h	Total Resistance ρ_t (Ohm.cm)
0	27.59
840	23.91
1200	22.10
2013	22.81
2896	27.01

Composition $Ce_{0.16}Y_{0.04}Sc_{0.6}Zr_{3.2}O_{7.68}$ has higher conductivity values than compositions with lower ceria content in the system, but after approximately 1800 h of this experiment conductivity has a rapid decrease, Fig. 2.

For the first 1080 h of the experiment, there is only one semi-circle, corresponding to the electrode process, no other processes were registered. After 2013 h, there is the appearance of a second semi-circle, which becomes more defined with the increase of time. After the appearance of this second semi-circle, total resistance rapidly increases. Capacitance values have the order of magnitude 10^{-8} F/cm and with time this value decreases. As this sample is well sintered; therefore the semi-circle could correspond to a grain boundary component [13, 14]. Values for total, bulk and grain boundary resistance are presented in Table IV. Bulk and grain boundary resistance increase significantly after 2440 h. This can indicate degradation of the grain boundary and/or a change in the microstructure of the grain boundary, after 2013 h, leading to an ageing and an increase in resistance.

There is a decrease in the total resistance from 0 h to 2013 h, as curves are located in the left side of the curve for 0 h. The measurement at 2896 h shows that total resistance has increased since the measurement at 2013 h. After 2013 h, resistance increases indicating ageing of the sample.

Comparison between compositions

There is a pattern which occurs for all compositions analysed, until 1800 h, conductivity is fairly stable; after 1800 h, conductivity decreases until the end of the experiment, indicating ageing. This is in agreement with Haering *et al*. [9] and Nomura *et al*. [15], who state that compositions with scandia content lower than 11 mol%, present degradation in conductivity in first the 500 h but when scandia content is higher than 11 mol% no degradation is observed in the first 500 h. The total dopant content is higher than 11 mol% for all compositions in the system.

The resistance of the composition $Ce_{0.04}Y_{0.16}Sc_{0.6}Zr_{3.2}O_{7.62}$ slightly decreases until 1800 h but after this time the resistance starts to increase. When a measurement is taken at 2896 h a semi-circle appears and it is possible to obtain values for bulk and grain boundary resistances. The composition $Ce_{0.16}Y_{0.04}Sc_{0.6}Zr_{3.2}O_{7.68}$ has a slight decrease of resistance until 1800 h; after this time the resistance starts to increase. From 2013 h until 2440 h the resistance increases slowly, but after this time, at 2896 h, the bulk and grain boundary resistances increase significantly. *"This is most likely that an ordering process and the formation of microdomains in the low temperature range during long annealing is responsible for conductivity degradation in cubic phase samples"*, as stated by Politova *et al*. [16]. For the composition $Ce_{0.20}Sc_{0.6}Zr_{3.2}O_{7.70}$, there is a clear increase in resistance, after 2013 h, indicating ageing.

The effect which most contributes for the conductivity is the defect association, their concentration and their transformation. As these defects play a major role for the electrical conductivity, it will influence the conductivity degradation too. One way to promote conductivity is to increase the oxygen vacancy number, by doping zirconia with a trivalent oxide. However if the dopant concentration is high, it creates a high level of vacancies, which will rearrange, hindering conductivity. In addition, the increase of vacancies will create an electrostatic interaction between the oxygen vacancies and the dopant cations. This leads to an ordering of the cations during annealing causing the formation of anions microdomains, therefore causing conductivity degradation [9, 11, 15, 16].

Scanning electron microscopy micrographs, SEM

Fig. 6 is a micrograph of a sample after ac impedance measurements and etching; it is shown for comparison with Fig. 7. The samples used for micrographs in Figs. 7, 8 and 9 are the ones used for the ageing experiment. The information regarding Fig. 6 is presented in [12].

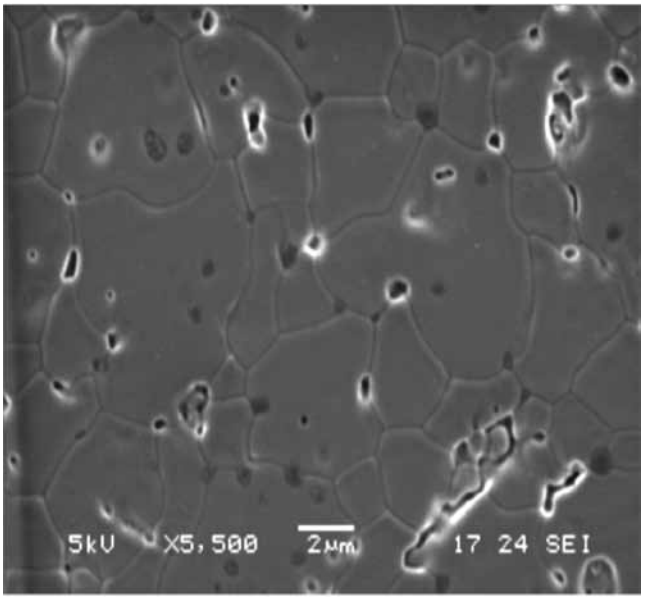

Figure 6: Scanning electron microscopy micrograph of $Ce_{0.04}Y_{0.08}Sc_{0.6}Zr_{3.2}O_{7.60}$, not aged.
[Figura 6: Fotografia do microscópio eletrônico de varredura da $Ce_{0,04}Y_{0,08}Sc_{0,6}Zr_{3,2}O_{7,60}$, não envelhecida.]

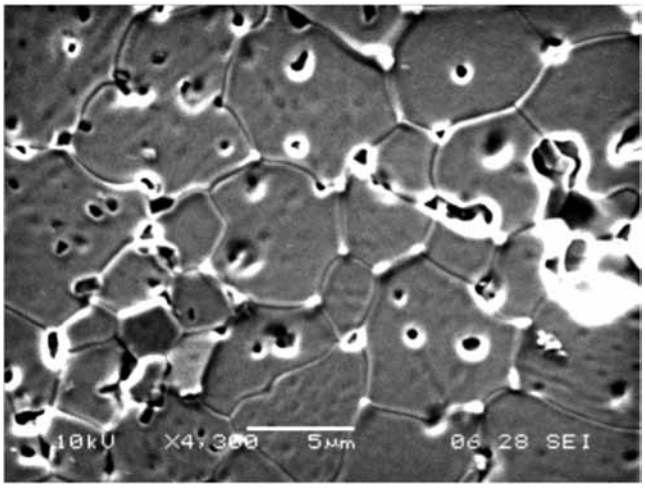

Figure 7: Scanning electron microscopy micrograph of $Ce_{0.04}Y_{0.08}Sc_{0.6}Zr_{3.2}O_{7.60}$, after ageing.
[Figura 7: Fotografia do microscópio eletrônico de varredura da $Ce_{0,04}Y_{0,08}Sc_{0,6}Zr_{3,2}O_{7,60}$, depois do envelhecimento.]

In Fig.7 grain boundaries are well defined and the hill and valley microstructure can be observed. In the sample with no ageing, Fig. 6, most pores are located in the grain boundary; while in sample after ageing, pores are observed within the grain, bulk. In the bottom left of Fig. 7, a region with some damage can be observed. There is also a darker colouration in Fig. 6 that does not appear in the sample after ageing, Fig. 7.

Fig. 8 shows grain boundaries are well defined but it looks that there are smaller grains inside larger ones. It has the appearance that grains start to be divided inside the larger grains. This could be the indication of microstructure ageing, therefore increasing the grain boundary resistance.

Fig. 8 shows significant damage on the surface, the hill and valley microstructure is more visible [17]. Cracks and fissures can be observed, showing microstructure deterioration of the sample.

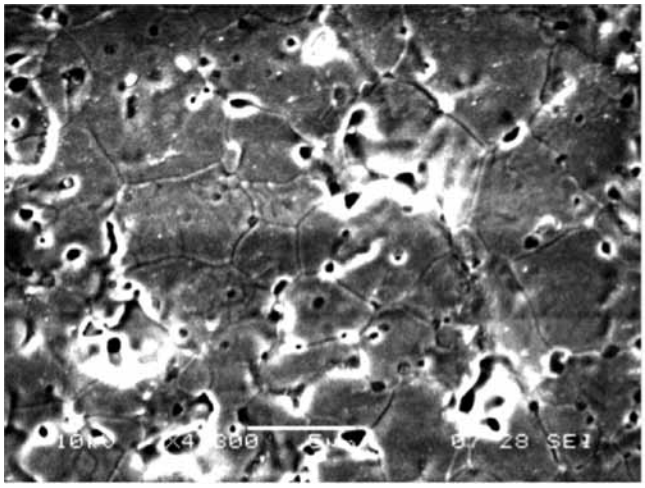

Figure 8: Scanning electron microscopy micrograph of $Ce_{0.16}Y_{0.04}Sc_{0.6}Zr_{3.2}O_{7.68}$, after ageing.
[Figura 8: Fotografia do microscópio eletrônico de varredura da $Ce_{0,16}Y_{0,04}Sc_{0,6}Zr_{3,2}O_{7,68}$, depois do envelhecimento.]

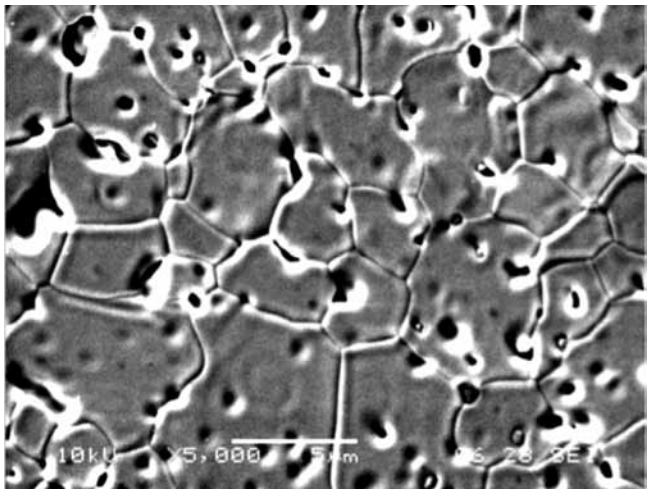

Figure 9: Scanning electron microscopy micrograph of $Ce_{0.2}Sc_{0.6}Zr_{3.2}O_{7.70}$, after ageing.
[Figura 9: Fotografia do microscópio eletrônico de varredura da $Ce_{0,2}Sc_{0,6}Zr_{3,2}O_{7,70}$, depois do envelhecimento.]

In Fig. 9 the hill and valley microstructure is visible [17], there are some irregularities on the surface and smaller grains are positioned inside the larger grains. When comparing micrographs with aged and not aged samples, the first observation is that grains with darker colouration do not appear on the aged samples. Visually, in aged samples, the surface seems to be irregular and damaged; in the microstructure there are cracks and fissures. In some cases, as for composition $Ce_{0.16}Y_{0.04}Sc_{0.6}Zr_{3.2}O_{7.68}$ shown in Fig. 8, damage is clearly visible. Smaller grains, with not well defined grain boundary, can be observed inside

larger grains with well defined grain boundaries. On the other hand, for compositions $Ce_{0.04}Y_{0.08}Sc_{0.6}Zr_{3.2}O_{7.60}$ and $Ce_{0.2}Sc_{0.6}Zr_{3.2}O_{7.70}$, Fig. 7 and Fig. 9, respectively, some damage on the surface can be observed, but not as extensive as in Fig. 8. The composition $Ce_{0.16}Y_{0.04}Sc_{0.6}Zr_{3.2}O_{7.68}$, Fig. 8, displays significant surface damage, which correlates with the appearance of a semi-circle for time equals 2013 h and from this time grain boundary resistance increases until the end of the experiment, Fig. 4 and Table IV.

Impedance spectra for composition $Ce_{0.2}Sc_{0.6}Zr_{3.2}O_{7.70}$, Fig. 5, do not show any semi-circle during all experiment, which correlates with a less damaged surface, Fig. 9.

CONCLUSIONS

For the first 1800 h all compositions present fairly stable conductivity values. After this time conductivity decreases; in some cases, compositions $Ce_{0.04}Y_{0.08}Sc_{0.6}Zr_{3.2}O_{7.60}$ and $Ce_{0.20}Sc_{0.6}Zr_{3.2}O_{7.70}$, this decreases is rapid. When micrographs from samples after ac impedance and samples after the ageing are compared, the first observation is that grains with darker colouration do not appear in the samples after ageing. The surface of samples after ageing has irregularities that are not present on the surface of samples after ac impedance. For all micrographs of samples after ageing, the grain boundaries are well defined and an increase of pores inside grains can be observed, in some cases the surface is damaged showing cracks and fissures. For all compositions, the hill and valley microstructure is visible [17]. For all composition there is an ageing due to rearrangement involving the defects introduced by dopants. These defects will order during long annealing, originating conductivity degradation.

ACKNOWLEDGEMENTS

We thank the RealSOFC EU integrated project for a travel grant that enabled this research to be performed. We acknowledge Supergen, EPSRC and Tim Worstall from TTE metals for scandia supply.

REFERENCES

[1] M. Yashima, M. Kakihana, M. Yoshimura, Solid State Ionics, **86-88** (1996) 1131.
[2] S. P. S. Badwal, F. T. Ciacchi, D. Milosevic, Solid State Ionics **136-137** (2000) 91.
[3] K. Eguchi, N. Akasaka, H. Mitsuyaser, Y. Nonaka, Solid State Ionics **135** (2000) 589.
[4] N. Minh, J. Am. Ceram. Soc. **76**, 3 (1993) 563.
[5] Y. Murakami, I. Nagano, H. Yamamoto, J. Mater. Sci. Lett. **16** (1997) 1686.
[6] S. P. S. Badwal, Solid State Ionics **52** (1992) 23.
[7] F. T. Ciacchi, S. P. S. Badwal, J. Eur. Ceram. Soc. **7** (1991) 197.
[8] T. S. Zhang, J. Ma, L. B. Kong, S. H. Chan, J. A. Kilner, Solid State Ionics **170** (2004) 209.
[9] C. Haering, A. Roosen, H. Schichl, M. Schnoeller, Solid State Ionics **176** (2005) 261.
[10] F. T. Ciacchi, S. P. S. Badwal, J. Drennan, J. Eur. Ceram. Soc. **7** (1991) 185.
[11] C. Haering, A. Roosen, H. Schichl, Solid State Ionics **176** (2005) 253.
[12] E. de Carvalho, W. Preis, W. Sitte, J. T. S. Irvine, Solid State Ionics **181** (2010) 1344 .
[13] J. T. S. Irvine, D. C. Sinclair, A. R. West, Adv. Mater. **2** (1990) 132.
[14] J. R. MacDonald, "Impedance Spectroscopy, emphasizing solid materials and systems", John Wiley & Sons, N. York, USA (1987).
[15] K. Nomura, Y. Mizutari, H. Kawai, Y. Nakamura, O. Yamamoto, Solid State Ionics **132** (2000) 235.
[16] T. Politova, J. T. S. Irvine, Solid State Ionics **168** (2004) 15.
[17] M. S. Schmidt, K. V. Hansen, K. Norman, M. Mogensen, Solid State Ionics **179** (2008)1436.
(Rec. 11/02/2011, Ac. 23/03/2011)